1 **Mangrove canopy height globally related to precipitation, temperature and cyclone**
2 **frequency**
3
4 Marc Simard*[1], Lola Fatoyinbo*[2], Charlotte Smetanka[1,3] , Victor H. Rivera-Monroy[4], Edward

5 Castañeda-Moya[4,5], Nathan Thomas[2,6], Tom Van der Stocken[1]

6

7 *Corresponding Authors: marc.simard@jpl.nasa.gov; lola.fatoyinbo@nasa.gov

8

9   1. Radar Science and Engineering Section, Jet Propulsion Laboratory, California Institute

10   of Technology, Pasadena, CA, USA

11   2. Biospheric Sciences Laboratory, NASA Goddard Space Flight Center, Greenbelt, MD,

12   USA

13   3. Université de Sherbrooke, Sherbrooke, Québec, Canada

14   4. Department of Oceanography and Coastal Sciences, College of the Coast and

15   Environment, Lousiana State University, Baton Rouge, LA, USA

16   5. Present address: Southeast Environmental Research Center, Florida International

17   Universiy, Miami, FL, USA

18   6. Earth System Science Interdisciplinary Center, University of Maryland, College Park,

19   MD, USA

20

21

22

24

25

26　　Mangrove wetlands are among the most productive and carbon-dense ecosystems in the

27　　world. Their structural attributes vary considerably across spatial scales, yielding large

28　　uncertainties in regional and global estimates of carbon stocks. Here, we present a global

29　　analysis of mangrove canopy height gradients and aboveground carbon stocks based on

30　　remotely sensed measurements and field data. Our study highlights that precipitation,

31　　temperature and cyclone frequency explain 74% of the global trends in maximum canopy

32　　height, with other geophysical factors influencing the observed variability at local and

33　　regional scales. We find the tallest mangrove forests in Gabon, equatorial Africa, where

34　　stands attain 62.8 m. The total global mangrove carbon stock (above- and belowground

35　　biomass, and soil) is estimated at 5.03 Pg, with a quarter of this value stored in Indonesia.

36　　Our analysis implies sensitivity of mangrove structure to climate change, and offers a

37　　baseline to monitor national and regional trends in mangrove carbon stocks.

38

39

40

41

42

43

44

45

46

47

48   Mangroves are forested wetlands that represent a functional link between the terrestrial and

49   oceanic carbon cycles[1], storing up to four times as much carbon per unit area in comparison to

50   terrestrial forest ecosystems[2]. Mangroves contribute an estimated 10–15% of the global carbon

51   storage in the coastal ocean, with ca. 50% of mangrove litterfall production being transported to

52   adjacent coastal zones and accounting for 10–11% of the global export of particulate terrestrial

53   carbon to the ocean[3,4]. Furthermore, mangrove forests provide a wealth of ecosystem services to

54   coastal communities including habitat for fisheries, firewood and timber, all valuable resources in

55   local markets[5]. Despite this, mangroves are impacted by anthropogenically driven disturbances

56   such as deforestation, conversion to aquaculture and urban development[6–8], and coastline

57   transgression due to relative sea level rise[9,10,11]. Recent estimates of global mangrove loss rates

58   range between 0.16% and 0.39% annually, and may be up to 8.08% in Southeast Asia[12]. As a

59   consequence, large amounts of previously stored carbon may be released into the atmosphere,

60   contributing substantially to net global carbon emissions[13–15].

61   Global mangrove carbon stocks[2] and aboveground biomass (AGB)[16,17] have been estimated

62   previously, providing AGB values derived from climate-based[16] or latitudinal relationships[17]. The

63   spatially explicit distribution in forest structural attributes such as mangrove canopy height is

64   rarely considered in these estimates. Mangrove canopy height is highly correlated with carbon

65   turnover via leaf or litterfall production[18] and is therefore an important variable in quantifying

66   contemporary global aboveground productivity and carbon sequestration rates. Productivity and

67   forest structure are controlled by local environmental gradients (e.g., nutrient availability, salinity)

68   and hydrology[19,20], along with regional climate and geomorphology[17,19–22], resulting in a range of

69   mangrove ecotypes, from scrub (< 3 m) to tall (> 15 m) forest stands[23–25]. Here, we produced global

70   maps of mangrove canopy height and AGB derived from spaceborne remote sensing data and *in*

71   *situ* measurements, to perform a global analysis of the spatial patterns and variability in mangrove

72   forest structure.

73

74   **Global distribution of mangrove canopy height**

75   We used the global mangrove extent map[26], the Shuttle Radar Topography Mission (SRTM) 30 m

76   resolution global Digital Elevation Model, and Geoscience Laser Altimeter System (GLAS) global

77   Lidar altimetry products, to produce two baseline canopy height maps for the year 2000: a map of

78   maximum canopy height (i.e., height of the tallest tree; Fig. 1) and a map of basal area weighted

79   height (i.e., individual tree heights weighted in proportion to their basal area). The latter map was

80   only used to generate the aboveground mangrove biomass map (see Methods). Our analysis of

81   mangrove canopy height distribution is based on the maximum canopy height map. Both maps

82   were validated using *in situ* field measurements of tree height from 331 plots (Supplementary

83   Table 1), resulting in an overall root mean square error of 3.6 m and 6.3 m respectively

84   (Supplementary Fig. 1). The maximum canopy height map shows that half of the world's

85   maximum mangrove canopy height is shorter than 13.2 m (Fig. 2). Maximum canopy height

86   exceeds 62 m ± 6.8 m (Fig. 2), rivaling maximum tree heights found in upland tropical forests[27].

87   Equatorial regions of the West African and South American coasts stand out as hotspots with the

88   tallest mangroves (Table 1a; Supplementary Tables 2–6). The top five countries (Table 1a) with

89   the tallest mangroves are: Gabon (62.8 m; Fig. 3), Equatorial Guinea (57.7 m), Colombia (54.3

90   m), Venezuela (52.6 m), and Panama (50.9 m). These productive forests are significantly taller

91   than previously reported values[16,18,28] and are located in estuarine environments of the world's most

92   remote, cloudiest, wettest (precipitation > 500 cm yr^{-1}), and hottest regions (mean air temperature

93   25.6 °C; ref. [29]). In addition, these wetlands grow in river-dominated coastal settings with low

94 human population densities, potentially high nutrient availability, reduced soil salinity values, and

95 significant protection from cyclone-induced high-energy winds and waves[17,30].

96   We analyzed global trends in mangrove canopy height with latitude, cyclone landfall

97 frequency, precipitation, temperature, sea surface salinity (SSS), and tidal range. Globally, the

98 distribution of maximum mangrove canopy height follows a Gaussian latitudinal trend ($R^2 = 0.91$),

99 peaking at 1.13° N (Fig. 4a), similar to trends of precipitation and temperature. The global

100 distribution of canopy height suggests that cyclone landfall frequency may limit the growth of

101 mangrove forests (Fig. 4a). Cyclone disturbance has been shown to be important at more regional

102 scales[31]. However, their impact may be confounded by other environmental factors (Fig. 4b). Our

103 results indicate that coastline-specific trends in maximum canopy height reflect the important role

104 of precipitation (Fig. 4b) in controlling mangrove structure and distribution, as shown recently by

105 Osland and colleagues[32]. For example, the trends reflect similar differences between the East and

106 West coasts of the Americas and Africa. While large-scale SSS appears to align with mangrove

107 canopy height (Fig. 4b), the explanatory role of this factor remains unclear as it varies strongly

108 over short distances in estuarine environments, and is regulated by precipitation,

109 evapotranspiration, riverine input, and ocean circulation[33]. We did not find a significant

110 relationship of canopy height variability with local tidal range (see Methods; Supplementary Fig.

111 2). A multivariate regression analysis shows that annual precipitation, mean temperature and

112 tropical cyclone landfall frequency explain 74% of latitudinal trends in maximum mangrove

113 canopy height (see Methods; Supplementary Table 7).

114   The spatial variability in canopy height also reflects the role of local-scale geophysical

115 factors driving environmental gradients within distinct ecogeomorphic settings (e.g., nutrient

116 availability and soil pore water salinity)[20,34]. For instance, where we located the tallest mangrove

117　canopy height in the upper Gabon estuary (Africa; Fig. 3), we also detected low stature mangrove

118　wetlands near the mouth of the same estuary (see also ref. [35]). The relative influence of regional

119　and local factors within a given latitude hosting a diversity of ecogeomorphic settings[17] determines

120　not only the species-specific mangrove spatial distribution in a given coastal region, but also the

121　spatial distribution of above- and belowground biomass allocation patterns regardless of latitude[36].

122　However, quantifying the relative contributions of these factors to the global variability observed

123　in our canopy height map is beyond the scope of this study, particularly because they currently

124　cannot be resolved by remote sensing measurements. Instead, our maps can help define research

125　agendas and field campaigns to quantify the relative contribution of local drivers such as

126　hydroperiod, a critical factor controlling nutrient availability and soil salinity in mangrove

127　wetlands[24].

128

Global trends of mangrove biomass and carbon stocks

130　Much attention is given to mangrove forests due to their significant allocation of carbon

131　belowground[2,3,36–39]. However, carbon sequestration rates are estimated by using wood production

132　and litterfall rates that are positively correlated with tree height and AGB[9,18]. We developed and

133　validated regional and global AGB models (Supplementary Table 8) from 331 field plots

134　distributed across 3 continents (Fig. 1), spanning 51 degrees in latitude and 168 degrees in

135　longitude (see Methods).

136　　　Our maps indicate that mangroves can store substantial aboveground carbon stocks

137　(maximum AGB of 910.5 Mg ha^{-1} ± 84.2 Mg ha^{-1}; Table 1a), and show considerable spatial

138　variability. Similar to canopy height, the global distribution of AGB maxima in mangrove forests

139　follows a Gaussian latitudinal trend with a peak near 0.47° S (Supplementary Fig. 3). The top five

140 countries in terms of total AGB are (Table 1b): Indonesia (574.3 Tg, 2.7 Mha), Papua New Guinea

141 (114.0 Tg, 0.5 Mha), Australia (112.8 Tg, 0.9 Mha), Brazil (97.8 Tg, 1.1 Mha), and Malaysia (95.6

142 Tg, 0.6 Mha). These countries are characterized by vast expanses of mangrove forests and a high

143 proportion of tall stands. The top-ten list (Table 1b) differs from previously reported rankings that

144 include Indonesia and Papua New Guinea, but not Bangladesh, Myanmar, Venezuela, and

145 Cameroon[16]. Furthermore, our field dataset underscores major regional differences in allometric

146 relationships between canopy height and AGB (Supplementary Fig. 4, Supplementary Table 8).

147 For example, our allometric model for East African coastal regions derived from *in situ* data shows

148 that, for the same forest canopy height, AGB in East Africa is significantly higher than in the

149 Americas. This difference in values highlights the relative importance of tree density[40] when

150 calculating AGB in sites within the same latitude, and the need to develop regional allometry

151 covering a wide range of environmental settings.

152   When adding our global aboveground carbon stock value to recently published values for

153 average organic soil carbon stock (283 Mg C ha^{-1}; see ref. [41]) and root biomass (from allometric

154 models; see ref. [42]), we obtain a total global carbon stock estimate of 5.03 Pg, of which nearly a

155 quarter (22.7%) is stored in Indonesia (see Supplementary Tables 2–6 for the per country and per

156 continent overview). Our estimate is in line with recently published total carbon stock estimates

157 (Supplementary Table 9), in part due to the significant contribution of belowground carbon to the

158 total global carbon estimate.

159   While our estimates of total global AGB (1.75 Pg) and mean AGB density (129.1 Mg ha^{-1}

160 ± 87.2 Mg ha^{-1}) are significantly lower than previously reported by Hutchison and colleagues[16]

161 (2.83 Pg and 184.8 Mg ha^{-1}, respectively), our total is close to the mean (1.88 Tg) of a range of

162 published values (Supplementary Table 9). The difference in estimates is primarily due to

163   methodological approaches such as the use of different mangrove extent maps. Additionally, a few

164   previous AGB estimates, such as the one of Hutchison and colleagues[16], represent the *potential*

165   AGB obtained by modeling biomass based on latitude[43,44] and bioclimatic variables[16]. In contrast,

166   our estimate is based on *direct* measurements of canopy height from spaceborne Radar and Lidar

167   instruments, coupled with extensive *in situ* forest structure and composition measurements. As

168   such, the differences between our estimates and those reported in previous studies reflect local-

169   scale variability within mangrove forests and areas where mangroves are stressed or impacted by

170   environmental and geophysical factors, and anthropogenic activity. For example, differences of

171   mean AGB between studies (here shown as 'satellite-based' from this study vs 'environmental

172   model' from ref. [16]) in West Africa are: Benin (10.0 Mg ha^{-1} vs 160.6 Mg ha^{-1}), Ghana (59.8 Mg

173   ha^{-1} vs 166.9 Mg ha^{-1}), Nigeria (96.5 Mg ha^{-1} vs 195.1 Mg ha^{-1}), Sierra Leone (74.7 Mg ha^{-1} vs

174   180.2 Mg ha^{-1}), and The Gambia (42.0 Mg ha^{-1} vs 144.9 Mg ha^{-1}), suggesting that model-based

175   estimates may have overestimated AGB by 100 Mg ha^{-1} or more. Mangrove wetlands in these

176   regions are heavily impacted by anthropogenic pressures such as wood harvesting, bio-fuel

177   plantations, development projects, and industrial pollution[45], and may explain discrepancies.

178   Industrial pollution, for example, is a common cause of mangrove degradation in the Niger Delta

179   region (Nigeria)[46]. Similarly, our total carbon estimate for Indonesia (1141 TgC) is less than half

180   of that reported by Murdiyarso and colleagues[7] (3140 TgC). This discrepancy is due to differences

181   in the soil depth (1 m in this study; 2–3m in Murdiyarso et al.[7]) that is being considered for

182   estimating the soil carbon component and our use of a smaller total mangrove area (2.7 Mha vs

183   4.2 Mha). These findings also suggest that regions with deep carbon-rich soils can potentially yield

184   higher values than those reported in this study. While we report on the top 1 m of soil as a first-

185   order conservative estimate, we foresee the continued development of more spatially-explicit maps

186   of soil carbon in blue carbon ecosystems[36,37,47] that can be coupled with our AGB and carbon

187   datasets.

188

189   **Baseline for monitoring regional and global carbon trends**

190   In this study, we have shown that mangroves can store substantial aboveground carbon

191   stocks and that continental to global patterns of mangrove canopy height and AGB follow

192   precipitation, temperature, and cyclone landfall frequency trends. Moreover, our spatially explicit

193   maps indicate that local-scale geophysical and environmental conditions also regulate forest

194   structure and therefore carbon stocks and sequestration rates. Our mangrove canopy height map

195   revealed a vast range of canopy heights, including maximum realized values (> 62 m) that surpass

196   maximum heights of other forest types worldwide[27], and the discovery of the tallest stands of

197   mangrove forests in the world, on the Atlantic coast of Central Africa, and the Pacific coast of

198   South America. Our AGB map can serve as a baseline input for estimating the contribution of

199   mangroves to carbon sequestration by wetlands in general and the potential contribution of CO_2

200   emissions resulting from mangrove degradation and loss[15,39, 43].

201

202   # References

203   1. McLeod, E. et al. A blueprint for blue carbon: toward an improved understanding of the role

204   of vegetated coastal habitats in sequestering CO_2. *Front. Ecol. Environ.* **9**, 552–560 (2011).

205   2. Donato, D. C. et al. Mangroves among the most carbon-rich forests in the tropics. *Nat.*

206   *Geosci.* **4**, 293–297 (2011).

207   3. Alongi, D. M. Carbon cycling and storage in mangrove forests. *Annu. Rev. Mar. Sci* **6**, 195–

208   219 (2014).

209 4. Bouillon, S. et al. Mangrove production and carbon sinks: a revision of global budget

210   estimates. *Global Biogeochem. Cycles* **22**, GB2013 (2008).

211 5. Barbier, E. B. et al. The value of estuarine and coastal ecosystem services. *Ecol. Monogr.* **81**,

212   169–193 (2011).

213 6. Polidoro, B. A. et al. The loss of species: mangrove extinction risk and geographic areas of

214   global concern. **5**, e10095 (2010).

215 7. Murdiyarso, D. et al. The potential of Indonesian mangrove forests for global climate change

216   mitigation. *Nat. Clim. Chang.* **5**, 8–11 (2015).

217 8. Richards, D. R. & Friess, D. A. Rates and drivers of mangrove deforestation in Southeast

218   Asia, 2000-2012. *Proc. Natl. Acad. Sci.* **113**, 344–349 (2016).

219 9. Krauss, K. W. et al. How mangrove forests adjust to rising sea level. *New Phytol.* **202**, 19–34

220   (2014).

221 10. Lovelock, C. et al. The vulnerability of Indo-Pacific mangrove forests to sea-level rise.

222   *Nature* **526**, 559–563 (2015).

223 11. Sasmito, S. D., Murdiyarso, D., Friess, D. & Kurniato, S. Can mangroves keep pace with

224   contemporary sea level rise? A global data review. *Wetlands Ecol. Manage.* **24**, 263–278

225   (2016).

226 12. Hamilton, S. E. & Casey, D. Creation of a high spatio-temporal resolution global database of

227   continuous mangrove forest cover for the 21st century (CGMFC-21). *Glob. Ecol. Biogeogr.*

228   **25**, 729–738 (2016).

229 13. Lovelock, C. E., Reuss, R. W. & Feller, I. C. CO_2 efflux from cleared mangrove peat. *PLoS*

230   *ONE* **6**, e21279 (2011).

231 14. Kauffman, J. B., Heider, C., Norfolk, J. & Payton, F. Carbon stocks of intact mangroves and

232   carbon emissions arising from their conversion in the Dominican Republic. *Ecol. Appl.* **24**,

233   518–527 (2014).

234   15. Hamilton, S. E. & Friess, D. A. Global carbon stocks and potential emissions due to

235   mangrove deforestation from 2000 to 2012. *Nat. Clim. Chang.* **8**, 240–244 (2018).

236   16. Hutchison, J., Manica, A., Swetnam, R., Balmford, A. & Spalding, M. Predicting global

237   patterns in mangrove forest biomass. *Conserv. Lett.* **7**, 233–240 (2014).

238   17. Rovai, A. S. et al. Scaling mangrove aboveground biomass from site-level to continental-

239   scale. *Glob. Ecol. Biogeogr.* **25**, 286–298 (2016).

240   18. Saenger, P. & Snedaker, S. C. Pantropical trends in mangrove above-ground biomass and

241   annual litterfall. *Oecologia* **96**, 293–299 (1993).

242   19. Twilley, R. R. & Rivera-Monroy, V. H. in *Coastal Wetlands: An Integrated Ecosystem*

243   *Approach.* (eds. Perillo, G. M. E., Wolanski, E., Cahoon, D. R. & Brinson, M. M.) Ch. 23

244   (Elsevier, Amsterdam, 2009).

245   20. Thom, B. G. in *Mangrove ecosystems in Australia* (ed. Clough, B. F.) 3–17 (Australian

246   National University Press, Canberra, 1982).

247   21. Danielson, T. M. et al. Assessment of Everglades mangrove forest resilience: implications for

248   above-ground net primary productivity and carbon dynamics. *Forest Ecol. Manag.* **404**, 115–

249   125 (2017).

250   22. Twilley, R. R., Castaneda-Moya, E., Rivera-Monroy, V. H. & Rovai, A. S. in *Mangrove*

251   *Ecosystems: A Global Biogeographic Perspective. Structure, Function, and Services.* (eds.

252   Rivera-Monroy, V. H., Lee, S. Y., Kristensen, E. & Twilley, R. R.) Ch. 5 (Springer,

253   Switzerland, 2017).

254   23. Simard, M., Rivera-Monroy, V. H., Mancera-Pineda, J. E., Castañeda-Moya, E. & Twilley,

255   R. R. A systematic method for 3D mapping of mangrove forests based on Shuttle Radar

256   Topography Mission elevation data, ICEsat/GLAS waveforms and field data: application to

257   Ciénaga Grande de Santa Marta, Colombia. *Remote Sens. Environ.* **112**, 2131–2144 (2008).

258 24. Castañeda-Moya, E., Twilley, R. R. & Rivera-Monroy, V. H. Allocation of biomass and net

259   primary productivity of mangrove forests along environmental gradients in the Florida

260   coastal Everglades, USA. *For. Ecol. Manage.* **307**, 226–241 (2013).

261 25. Balke, T. & Friess, D. A. Geomorphic knowledge for mangrove restoration: a pan-tropical

262   categorization. *Earth Surf. Process. Landforms* **41**, 231–239 (2016).

263 26. Giri, C. et al. Status and distribution of mangrove forests of the world using earth observation

264   satellite data. *Glob. Ecol. Biogeogr.* **20**, 154–159 (2011).

265 27. Simard, M., Pinto, N., Fisher, J. B. & Baccini, A. Mapping forest canopy height globally

266   with spaceborne lidar. *J. Geophys. Res. Biogeosci.* **116**, 1–12 (2011).

267 28. Pan, Y., Birdsey, R. A., Phillips, O. L. & Jackson, R. B. The Structure, distribution, and

268   biomass of the world's forests. *Annu. Rev. Ecol. Evol. Syst.* **44**, 593–622 (2013).

269 29. Hijmans, R. J., Cameron, S. E., Parra, J. L., Jones, P. G. & Jarvis, A. Very high resolution

270   interpolated climate surfaces for global land areas. *Int. J. Climatol.* **25**, 1965–1978 (2005).

271 30. Ward, R. D., Friess, D. A., Day, R. H. & MacKenzie, R. A. Impacts of climate change on

272   mangrove ecosystems: a region by region overview. *Ecosyst. Health Sustainability* **2**, e01211

273   (2016).

274 31. Farfán, L. M., D'Sa, E. J., Liu, K.-b. & Rivera-Monroy V. H. Tropical cyclone impacts on

275   coastal regions: the case of the Yucatán and the Baja California Peninsulas, Mexico. *Estuar.*

276   *Coasts* **37**, 1388–1402 (2014).

277 32. Osland, M. J. et al. Climatic controls on the global distribution, abundance, and species

278   richness of mangrove forests. *Ecol. Monogr.* **87**, 341–359 (2017).

279   33. Terray, L. et al. Near-surface salinity as nature's rain gauge to detect human influence on the

280   tropical water cycle. *J. Clim.* **25**, 958–977 (2012).

281   34. Twilley, R. R. in *Maximum Power: the Ideas and Applications of H.T. Odum* (ed. Hall,

282   C.A.S.) 43–62 (University Press of Colorado, Niwot, Colorado, 1995).

283   35. Kauffman, J. B. & Bhomia, R. K. Ecosystem carbon stocks of mangroves across broad

284   environmental gradients in West-Central Africa: global and regional comparisons. *PLoS*

285   *ONE* **12**, e0187749 (2017).

286   36. Rovai, A. S. et al. Global controls on carbon storage in mangrove soils. *Nat. Clim. Change* **8**,

287   534–538 (2018).

288   37. Sanderman, J. et al. A global map of mangrove forest soil carbon at 30 m spatial resolution.

289   *Environ. Res. Lett.* **13**, 055002 (2018).

290   38. Bouillon, S. Carbon cycle: storage beneath mangroves. *Nat. Geosci.* **4**, 282–283 (2011).

291   39. Lovelock, C. E. et al. Assessing the risk of carbon dioxide emissions from blue carbon

292   ecosystems. *Front. Ecol. Environ.* **15,** 257–265 (2017).

293   40. Fatoyinbo, T., Feliciano, E. A., Lagomasino, D., Lee, S. K. & Trettin, C. Estimating

294   mangrove aboveground biomass from airborne LiDAR data: a case study from the Zambezi

295   River delta. *Environ. Res. Lett.* **13**, 025012 (2017).

296   41. Atwood, T. B. et al. Global patterns in mangrove soil carbon stocks and losses. *Nat. Clim.*

297   *Chang.* **7**, 523–528 (2017).

298   42. Chave, J. et al. Tree allometry and improved estimation of carbon stocks and balance in

299   tropical forests. *Oecologia* **145**, 87–99 (2005).

300   43. Siikamäki, J., Sanchirico, J. N. & Jardine, S. L. Global economic potential for reducing

301   carbon dioxide emissions from mangrove loss. *Proc. Natl. Acad. Sci.* **109**, 14369–14374

302   (2012).

303   44. Twilley, R. R., Chen, R. H. & Hargis, T. Carbon sinks in mangroves and their implications to

304   carbon budget of tropical coastal ecosystems. *Water Air Soil Poll.* **64**, 265–288 (1992).

305   45. Feka, N. Z. & Ajonina, G. N. Drivers causing decline of mangrove in West-Central Africa: a

306   review. *Int. J. Biodiv. Science Ecosys. Serv. Manag.* **7**, 217–230 (2011).

307   46. Omo-Irabor, O. O. et al. Mangrove vulnerability modelling in parts of Western Niger Delta,

308   Nigeria using satellite images, GIS techniques and Spatial Multi-Criteria Analysis (SMCA).

309   *Environ. Monit. Assess.* **178**, 39–51 (2011).

310   47. Hinson, A. L. et al. The spatial distribution of soil organic carbon in tidal wetland soils of the

311   continental United States. *Glob. Chang. Biol.* **23**, 5468–5480 (2017).

312

Author contributions

M.S. and L.F. conceived and designed the study. M.S. led the SRTM and ICESat/GLAS data processing, with assistance from C.S., L.F. and N.T. Field data processing and biomass model development was led by L.F., with assistance from M.S. Field experimental design and data collection was carried out by M.S., L.F., V.R-M, E.C-M. and N.T. The interpretation of data and generation of results were performed by M.S., L.F., C.S., V.R-M, E.C-M., T.V.D.S and N.T. The writing of the paper was led by M.S and L.F. with input from all co-authors.

Corresponding authors

Marc Simard Marc.Simard@jpl.nasa.gov and Lola Fatoyinbo Lola.fatoyinbo@nasa.gov

Methods

Mangrove canopy height estimation with SRTM and ICESat/GLAS. The global maps of canopy height were generated using SRTM digital elevation model (DEM) data[48] collected in

370 February 2000 and Lidar heights from the ICESat/GLAS Spaceborne Lidar mission following a

371 methodology that was successfully implemented on regional scales in Florida, Colombia, and

372 across Africa, with RMSE values of 3 m or lower across the 1–30 m mean height range[23,49–51]. The

373 SRTM DEM values report elevations located at the InSAR scattering phase height center, which

374 corresponds to a height located in between the ground elevation and the top of the canopy[23,49,52] in

375 vegetated areas. This is due to radar microwaves penetrating and interacting within the forest

376 canopy, rather than with the top of the canopy or ground alone. To identify mangrove areas and

377 mask non-mangrove regions in the SRTM elevation dataset, we used the global mangrove extent

378 map from Giri and colleagues[26]. We only included areas with SRTM elevation values ranging from

379 0 to 55 m above mean sea level to remove some areas falsely identified as mangroves in the Giri

380 et al.[26] map. This threshold value preserves the tallest mangrove forest stands (Fig. 3). This map

381 was preferred over the more recent map developed by Hamilton and Casey[12] as it is coincidental

382 with the SRTM dataset (i.e., they are both from 2000), and to this date, it is the only one that

383 specifically maps mangroves from Landsat data, as opposed to using global canopy cover from

384 the Global Forest Change product[53].

385   GLAS Lidar altimetry data were collected globally from 2003 to 2009, providing the only

386 global Lidar canopy and height measurement, with sparse samples distributed across the globe.

387 We used GLAS data to remove the elevation bias introduced by the limited penetration of the

388 SRTM C-band microwave signal within the forest canopy, which allows for the spatially

389 comprehensive and accurate mapping of canopy height[51]. The GLAS Lidar-derived maximum

390 canopy height is defined as the height of the Lidar pulse containing all its energy between the

391 ground and the top of the tallest tree (i.e., referred to as the Relative Height of the 100th percentile,

392 RH100). We found a total of 57,369 Lidar waveforms in mangrove areas using the entire GLAS

393   archive spanning 2003 through 2009, filtering out the low quality measurements[27] and intersecting

394   the GLAS estimates of maximum canopy height with the SRTM mangrove extent subset.

395   Supplementary Fig. 5 shows the scatterplot of RH100 and SRTM elevation in mangrove areas. We

396   applied the regression model (1) relating GLAS RH100 to SRTM elevation measurements

397   (Supplementary Fig. 5) to obtain a global map of maximum canopy height:

398    $$SRTMH_{max} = 1.697 * H_{SRTM} \tag{1}$$

399   where H_{SRTM} represents the original SRTM DEM, and $SRTMH_{max}$ is the new maximum canopy

400   height dataset. Regions with an SRTM elevation of 0 m but mapped as mangroves in the Giri et

401   al.[26] map were assigned a default value of 0.5 m (based on field observations) as these are most

402   likely scrub or low-density mangrove forests that could not be detected by SRTM. We computed

403   the mean and maximum $SRTMH_{max}$ values for each country, as shown in Supplementary Tables

404   2–6. In total, we report all of the results obtained for 117 countries and territories. We defined the

405   maximum $SRTMH_{max}$ as the 95th percentile value in each country to minimize the impact of canopy

406   height error reported from a potentially small number of misclassified pixels. For countries with

407   the tallest forests (> 40 m), we identified the exact location of these forest stands to visually

408   ascertain that each region included more than one pixel representing tall mangroves, and especially

409   to avoid confusing the maximum $SRTMH_{max}$ with local topographic features included within the

410   mangrove mask[26]. In countries and territories with small mangrove areas close to steep topography,

411   higher topographic areas inland from mangrove fringe were often falsely classified as mangroves.

412   In these cases, mostly occurring over islands such as Japan, Palau, Samoa, Solomon Islands and

413   Fiji, the use of the 95th percentile to determine $SRTMH_{max}$ did not suffice to remove outliers, and

414   we therefore do not report their maximum $SRTMH_{max}$ value (see Supplementary Tables 2–6).

415   Finally, the SRTM estimates of H_{max} (i.e. $SRTMH_{max}$ were validated with *in situ* measurements

416   of H_{max} with an R^2 of 0.73 and an RMSE of 6.31 m globally (Supplementary Fig. 1b). In February

417   of 2016, *in situ* measurements of H_{max} were collected in Pongara National Park (Fig. 3) to confirm

418   the validity of the tallest canopy height values in Gabon. Here, the heights of five of the tallest

419   observed trees were measured using a laser rangefinder confirming the location of the areas with

420   the tallest mangrove canopy in the world (with all 5 trees measuring between 62 m and 65 m; Fig.

421   3).

422   In addition to H_{max}, we also generated a map of H_{ba}, the basal area weighted height, which

423   was used as input for the aboveground biomass (AGB) map. We chose H_{ba} because it has a lower

424   RMSE for the height estimate (see Supplementary Fig. 1) and there was more field data available

425   for the biomass model generation (we did not have H_{max} values for the Bangladesh data). The

426   smaller RMSE is also expected as H_{ba} is, like biomass, a function of basal area. We calculated

427    $SRTMH_{ba}$, by relating field values of H_{ba} (as described in the section below) with SRTM DEM

428   elevations (see Supplementary Fig. 1):

429            $$SRTMH_{ba} = 1.0754 * H_{SRTM} \hspace{6cm} (2)$$

430   where H_{SRTM} represents the original SRTM DEM and $SRTMH_{ba}$ the new basal area weighted

431   canopy height dataset.

432

433   **Height uncertainty.** The combination of multiple datasets and the global approach of our

434   study inevitably introduces some degree of uncertainty in our results. In the case of mangrove

435   height, the $SRTMH_{ba}$ data had an RMSE of 3.6 m when compared to *in situ* H_{ba} measurements as

436   shown in Supplementary Fig. 1. This means that in any particular pixel, if our $SRTMH_{ba}$ map

437   indicates a 4 m mangrove forest, the *in situ* H_{ba} is likely to be between 0.4 m and 7.6 m. However,

438   the $SRTMH_{max}$ uncertainty is larger, as indicated by the regression with GLAS RH100 (RMSE of

439 5.7 m) (Supplementary Fig. 5) and *in situ* H_{max} (RMSE of 6.31 m). Nonetheless, both height

440 estimates are more accurate than the elevation errors reported for the global SRTM DEM[54] as we

441 are only studying relative height in flat coastal areas where the impacts of topography on the DEM

442 error are reduced. While our estimated height uncertainty is significant at the 30 m pixel scale, it

443 is random, and therefore our global data products allow for the analysis of canopy structure trends

444 at regional and continental scales.

445   The regression residuals between the SRTM height estimates, the GLAS RH100 or field

446 results originate from several sources of uncertainty, discrepancies in the spatial scale and the

447 timing of measurements. There are inherent system errors associated with the GLAS and SRTM

448 sensors, field measurement errors, geo-location errors, and discrepancies in spatial resolution[51]

449 between the 30 m SRTM pixel, the 70 m GLAS footprint, and the various plot sizes used in this

450 study. Additionally, these measurements were acquired over different periods (February 2000 for

451 SRTM; 2003–2009 for GLAS; 2004–2016 for field) and are therefore impacted by natural changes

452 in canopy structure over time. A detailed analysis of differences in canopy height obtained from

453 SRTM, Lidar and field measurements[52] showed that SRTM height is sufficiently constant over

454 time to measure canopy height in established mangrove forests.

455

456 ***In situ* forest height and biomass estimation.** Our selected field sites (331 plots in total) included

457 a wide variety of forest structure and mangrove ecotypes (e.g., scrub, fringe, riverine, basin) with

458 measured *in situ* tree heights ranging from 1 m to 65 m (see Supplementary Table 1). The

459 mangrove field sites were distributed along a latitudinal range from 26º S (Maputo Reserve,

460 Mozambique) to 25º N (Everglades, USA), encompassing the equatorial region (e.g., Chocó,

461 Colombia). Field data were used to estimate forest structure attributes (i.e., H_{ba} and H_{max} and

462   AGB). Most of the data were collected in field plots throughout the Americas and Africa, using

463   fixed or variable plot sizes[49] (Supplementary Fig. 4, Supplementary Table 1). Within variable

464   plots, trees are selected using a fixed-angle gauge. For each selected tree, we identified species,

465   and measured the diameter at breast height (DBH) and height using a laser rangefinder or

466   clinometer. Tree density (i.e., # stems) was estimated for each plot and expressed per unit area

467   (hectares). Generally, the plot size depended on the largest tree size at each forest site. For instance,

468   in Chocó (Colombia) where trees were very tall and tree density was low, we used a 25 m fixed-

469   radius plot, while on Inhaca Island (Mozambique) where trees were small and tree density was

470   high, plots had a 7.5 m radius. In the Zambezi River Delta (Mozambique) 40 plots of 0.52 ha were

471   sampled with subplots[55,56] that each have a radius ranging between 3 m and 5 m. On Inhaca Island

472   (Mozambique), we sampled 51 plots with a radius of 7.5 m (0.0176 ha)[50]. For all sites, we

473   computed field basal area weighted height H_{ba} as:

474   $$H_{ba} = \frac{\sum_i (\pi r_i^2 \cdot H_i)}{\sum_i (\pi r_i^2)},$$ (3)

475   where H_i and r_i are the height and the radius (i.e., DBH/2) of tree i, respectively, in meters.

476   H_{ba} accounts for tree size which means larger trees have a stronger impact on the forest height

477   estimate. H_{max} was defined as the height of the tallest tree within a plot. *In situ* data were collected

478   within the 15 years period after the SRTM data was obtained.

479

480   **Global trends in mangrove structure.** To test whether spatial trends in mangrove canopy

481   structure are associated with temperature, precipitation, and tidal range, we used the WorldClim[57]

482   model, and tidal outputs from the ocean model developed by Wang and colleagues[58]. The analysis

483   of canopy height trends with these climate and environmental variables (WorldClim annual mean

484   temperature, mean temperature of warmest quarter, standard deviation of monthly mean

485   temperature, mean of coldest quarter, annual precipitation and sea surface salinity (SSS)) was

486   performed by intersecting a circle with a radius of 10 km centered on the coastline with mangroves

487   every half degree in latitude and intersecting the coastline at least 20 km apart in the longitudinal

488   direction. Cyclone frequency and distribution from 1842 to 2016 was calculated from the NOAA

489   International Best Track Archive for Climate Stewardship (IBTrACS version 3 release 9). In this

490   dataset the tropical cyclone occurrences are shown as points along their path. To generate a

491   histogram of cyclone frequency and distribution, we computed the percentage of these points

492   overlapping with mangrove areas, adding a buffer zone of 1.5 degrees to the mangrove location.

493   The buffer zone was added to include all tropical cyclones potentially influencing mangrove

494   growth. Previous studies show that precipitation and temperature are climatic variables that

495   regulate mangrove ecosystem structure (e.g., height and biomass) and function (i.e.,

496   productivity)[17,18]. Tidal range is computed as the minimum and maximum sea surface height

497   considering annual variations of four semidiurnal constituents and four diurnal constituents. The

498   mean SSS as a function of latitude for each continental region (Fig. 4b) was generated using 44

499   monthly mean maps (from 2011 and 2015) from version 4 Aquarius CAP Level 3 product[59]. The

500   sampled environmental variables were averaged per 1 degree of latitude, ranging from –34 to 30

501   degrees. The occurrence of cyclones was counted per 1 degree interval. A multivariate regression

502   analysis demonstrated the significant relationships between some environmental variables and

503   mangrove structure (i.e., maximum height) (Supplementary Table 7). Initially, all aforementioned

504   variables were included in the analysis with insignificant (i.e., $P > 0.05$) and highly correlated

505   variables (for example, minimum temperature and mean temperature) gradually eliminated. Only

506   temperature, precipitation and cyclone landfall frequency remained, explaining 74% of observed

507   global trends in mangrove maximum canopy height (Supplementary Table 7). Further analysis

508   also showed that precipitation alone explained 57% of global canopy height trends while

509   temperature alone explained 53%. Together, precipitation and temperature explained 71% of

510   global canopy height trends. The multivariate regression and variance inflation factor (VIF)

511   calculation were performed using the python *statsmodels* module[60]. All of the remote sensing data

512   processing and analysis was carried out using the Python scripting language, Quantum

513   Geographical Information System (QGIS)[61], the Geospatial Abstraction Library (GDAL), the

514   Remote Sensing and GIS python library (RSGISLib)[62] and GNU Parallel[63].

515

516   **Global mangrove biomass allometry development.** We used the *in situ* field datasets to derive

517   stand-level allometry between AGB, basal area weighted height H_{ba}, and maximum canopy height

518   H_{max}. AGB was estimated for each individual tree tagged inside the plot, using regional or site-

519   specific allometric equations as described by previous studies[23,40,50,64]. We used the generalized

520   pantropical tree allometric model[65] with species-specific wood density from the global wood

521   density database[66] to calculate above- and belowground (root) biomass of individual trees (see

522   Supplementary Table 1). The sum of individual trees within the plot was then computed and

523   normalized, using plot sizes, to represent total forest stand AGB density in Mg ha^{-1}. We then

524   generated regional and global models between plot-level canopy height and plot-level AGB

525   density, where height and AGB relationships were fitted to the regression model:

526       $$AGB = a \cdot H_x^b \tag{4}$$

527   where H_x can represent either H_{ba} or H_{max}. The global model was generated using all of the plot

528   data (n = 331) and H_{ba} of the field data, while the regional models were generated for the Americas

529   (using data from Colombia, USA, Venezuela, Brazil, Costa Rica, Ecuador, Mexico, n = 81), East

530   Africa (using data from Mozambique, n = 101), and South Asia (using data from Bangladesh, n =

531   149).

532   The analysis of the field data and the allometric regression models between field height

533   and AGB confirmed that while canopy height alone explains most of the variability in AGB,

534   adding stem density or basal area to the model, as in the case of H_{ba}, and developing region-

535   specific regressions, improved the relationship (Supplementary Fig. 4). In addition, H_{ba} is

536   computed from multiple tree measurements that reduce systematic and random height

537   measurement error at the stand level as opposed to H_{max}, which is reported from a single tree

538   measurement. Supplementary Fig. 4 shows the relationship of AGB with H_{ba} on a global scale as

539   well as region-specific scales.

540   Three region-specific allometric models were derived from field data, for East Africa, the

541   Americas, and Middle East–Asia. For Southeast Asia and Australia, a published allometric model

542   was used[64]. Finally, for West Africa, we applied the global allometric equation, as no field data

543   was available to generate a regional allometry. The regional biomass allometric models developed

544   in this study have RMSE values ranging from 54.3 Mg ha^{-1} to 103.4 Mg ha^{-1}. All models generated

545   for this study are shown in Supplementary Fig. 4 and all models used in the study can be found in

546   the Supplementary Table 8.

547

548   **Large-scale AGB estimation with SRTM**. The global mangrove forest AGB map was generated

549   by linking the field-measured biomass-height allometry (described above) with SRTM estimates

550   of H_{ba} (i.e., *SRTMH$_{ba}$*). This procedure implies a two-step process where SRTM is converted to

551   *SRTMH$_{ba}$* and then to AGB using appropriate field-derived H_{ba} to AGB allometry (Supplementary

552   Table 8). This approach is meant to facilitate potential updates by the user community as more

553 regional height-to-biomass models are developed. Supplementary Fig. 1a shows the relationship

554 between SRTM elevation and field-measured canopy height data, used to convert SRTM elevation

555 to *SRTMH$_{ba}$*. Using this method, the predicted AGB was estimated with an accuracy of 84.2 Mg

556 ha^{-1} at the plot level (Supplementary Fig. 6).

557   Finally, total (above- and belowground) biomass and carbon stock estimates by country

558 were generated by summing all corresponding pixels, and accounting for belowground biomass

559 and soil carbon. We computed the total aboveground carbon stocks per country, assuming a

560 stoichiometric factor of 0.451 as the AGB conversion factor, following the IPCC guidelines[67]. We

561 also accounted for belowground carbon and root biomass using published allometric models[42,68].

562 It is important to note that all allometric equations are site-specific and extrapolation may result in

563 a bias. For instance, in the Florida Everglades, root biomass in scrub forests can be 3–4 times

564 higher compared to AGB[69]. Furthermore, most allometric models do not account for scrub forests,

565 thereby adding uncertainty to the AGB and total carbon estimates. Nevertheless, we believe to

566 have used the most complete datasets and the most accurate values currently available, which can

567 be updated as new global belowground data and new allometry become available. Country-wide

568 belowground carbon stocks were estimated with a mean of 283 MgC ha^{-1} within the top 1 m of

569 soils[41]. Total root biomass was estimated as 49% of the AGB following the IPCC guidelines[67].

570 These generic values, uncertainties in the allometric models, along with the uncertainty of 12% [26]

571 in the mangrove extent map, will propagate as a bias in country-wide totals.

572

573 **Data availability.** The data that support the findings of this study are available from the Oak

574 Ridge National Data Archive (ORNL DAAC; https://doi.org/10.3334/ORNLDAAC/1665)

575 as GEOTIFF files and as an online webmapping tool

576 (https://mangrovescience.earthengine.app/view/mangroveheightandbiomass). The *in situ* field data

577 that have not been previously published is also available through the ORNL DAAC as *.csv* files

578 listing individual tree measurements (link https://doi.org/10.3334/ORNLDAAC/1665). The

579 SRTM and ICESat/GLAS datasets used as input to generate the maps can be downloaded from

580 https://lta.cr.usgs.gov/SRTM and https://nsidc.org/data/icesat/data.html respectively. The global

581 mangrove map (Giri et al.[26]) is freely available at http://data.unep-wcmc.org/datasets/4. The

582 tropical cyclone and SSS data are available from NOAA archives https://data.nodc.noaa.gov/cgi-

583 bin/iso?id=gov.noaa.ncdc:C00834 (doi:10.7289/V5NK3BZP) and

584 https://podaac.jpl.nasa.gov/dataset/AQUARIUS_L3_SSS_CAP_MONTHLY_V4?ids=Platform

585 &values=AQUARIUS_SAC-D (doi: 10.5067/AQR40-3TMCS).

586 The WorldClim data are available at the http://worldclim.org/version2.

587

588 **Competing interests**

589 The authors declare no competing interests.

590

591 **References**

592 48. Farr, T. et al. The shuttle radar topography mission. *Rev. Geophys.* **45,** 1–33 (2007).

593 49. Simard, M. et al. Mapping height and biomass of mangrove forests in Everglades National

594   Park with SRTM elevation data. *Photogramm. Eng. Remote Sens.* **72,** 299–311 (2006).

595 50. Fatoyinbo, T. E., Simard, M., Washington-Allen, R. A. & Shugart, H. H. Landscape-scale

596   extent, height, biomass, and carbon estimation of Mozambique's mangrove, forests with

597   Landsat ETM+ and Shuttle Radar Topography Mission elevation data. *J. Geophys. Res.*

598   *Biogeosciences* **113**, 1–13 (2008).

599   51. Fatoyinbo, T. E. & Simard, M. Height and biomass of mangroves in Africa from

600   ICESat/GLAS and SRTM. *Int. J. Remote Sens.* **34**, 668–681 (2013).

601   52. Lagomasino, D., Fatoyinbo, T., Lee, S. & Feliciano, E. A. Comparison of mangrove canopy

602   height using multiple independent measurements from land, air, and space. *Remote Sens.* **8**,

603   327 (2016).

604   53. Hansen, M. C. et al. High- resolution global maps of 21st-century forest cover change.

605   *Science* **342**, 850–853 (2013).

606   54. Rodríguez, E., Morris, C. S. & Belz, E. A Global Assessment of the SRTM Performance.

607   *Photogramm. Eng. Remote Sens.* **72**, 249–260 (2006).

608   55. Stringer, C. E. et al. *The Zambezi River Delta Mangrove Carbon Project: A Pilot Baseline*

609   *Assessment for REDD + Reporting and Monitoring Final Report.* 1–56 (2014).

610   56. Trettin, C. C., Stringer, C. E. & Zarnoch, S. J. Composition, biomass and structure of

611   mangroves within the Zambezi River Delta. *Wetl. Ecol. Manag.* **24**, 173–186 (2015).

612   57. Fick, S. E. & Hijmans, R. J. WorldClim 2: new 1-km spatial resolution climate surfaces for

613   global land areas. *Int. J. Climatol.* **37**, 4302–4315 (2017).

614   58. Wang, X., Chao, Y., Shum, C. K., Yi, Y. & Fok, H. S. Comparison of two methods to assess

615   ocean tide models. *J. Atmos. Ocean. Technol.* **29**, 1159–1167 (2012).

616   59. Yueh, S. H., Tang, W., Hayashi, A. K. & Lagerloef, G. S. E. L-Band passive and active

617   microwave geophysical model functions of ocean surface winds and applications to Aquarius

618   retrieval. *IEEE Trans. Geosci. Remote Sens.* **51**, 4619–4632 (2014).

619   60. Seabold, S. & Perktold, J. Statsmodels: Econometric and statistical modeling with

620   python. *Proc. 9th Python Sci. Conf.* (2010).

621   61. QGIS Development Team (2018). QGIS Geographic Information System. Open Source

622   Geospatial Foundation Project. http://qgis.osgeo.org.

623   62. Bunting, P., Clewley, D., Lucas, R. M. & Gillingham, S. The Remote Sensing and GIS

624   Software Library (RSGISLib). *Comput. Geosci.* **62**, 216–226 (2014).

625   http://dx.doi.org/10.1016/j.cageo.2013.08.007.

626   63. Tange, O. (2018) GNU Parallel 2018, Mar 2018, ISBN 9781387509881,

627   https://doi.org/10.5281/zenodo.1146014.

628   64. Aslan, A., Rahman, A. F., Warren, M. W. & Robeson, S. M. Mapping spatial distribution and

629   biomass of coastal wetland vegetation in Indonesian Papua by combining active and passive

630   remotely sensed data. *Remote Sens. Environ.* **183**, 65–81 (2016).

631   65. Chave, J. et al. Improved allometric models to estimate the aboveground biomass of tropical

632   trees. *Glob. Chang. Biol.* **20**, 3177–3190 (2014).

633   66. Chave, J. et al. Towards a worldwide wood economics spectrum. *Ecol. Lett.* **12**, 351–366

634   (2009).

635   67. Hiraishi, T. et al. (eds). *2013 Supplement to the 2006 IPCC Guidelines for National*

636   *Greenhouse Gas Inventories: Wetlands. Methodological Guidance on Lands with Wet and*

637   *Drained Soils, and Constructed Wetlands for Wastewater Treatment.* (IPCC, Switzerland,

638   2014).

639   68. Komiyama, A., Ong, J. E. & Poungparn, S. Allometry, biomass, and productivity of

640   mangrove forests: A review. *Aquat. Bot.* **89**, 128–137 (2008).

641   69. Castañeda-Moya, E. et al. Patterns of root dynamics in mangrove forests along

642   environmental gradients in the Florida coastal Everglades, USA. *Ecosystems* **14**, 1178–1195
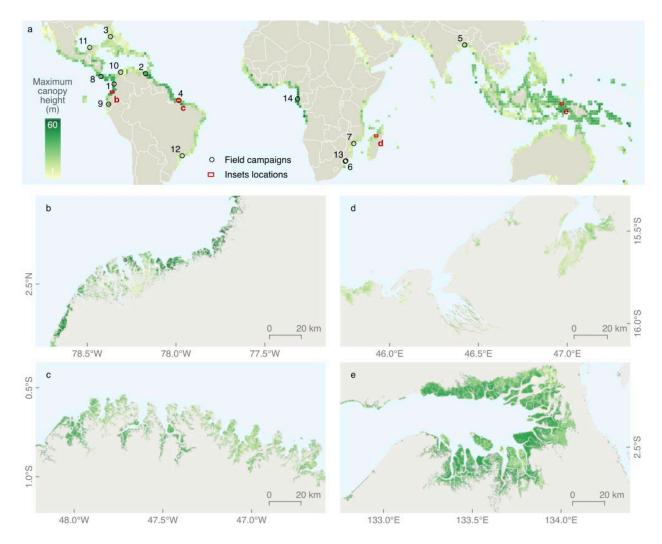
643   (2011).

644   **Figures**

645

646   **Figure 1 | Global map of mangrove maximum canopy height and location of sampling sites**

647   **(numbers) where *in situ* data were collected. a**, Green colors show tallest maximum mangrove

648   canopy height found within 1 degree cells. The map also shows the location of field sites and

649   high resolution insets for **b**, coastal Nariño and Cauca (Colombia); **c**, coastal Pará (Brazil); **d**,

650   Bombetoka Bay (Madagascar) and; **e**, Bintuni Bay (West Papua, Indonesia).
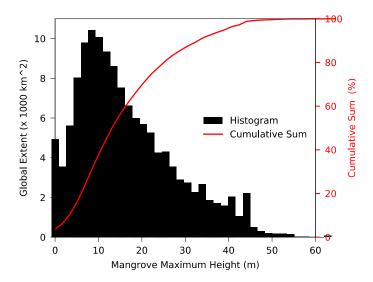
651

652

653

Figure 2 | Global distribution of maximum mangrove canopy height extent. Areal extent of forests within each height class at 1.7 m intervals (black) and cumulative sum of the percentages (red).

657

658

Figure 3 | Distribution of mangrove canopy height in the Gabon Estuary, on the Atlantic coast of Equatorial Africa. This map highlights the tallest mangrove forests globally with forest stands that were measured at 63 m on our map. The photo insets show locations where individual trees were measured *in situ* up to 65 m tall.
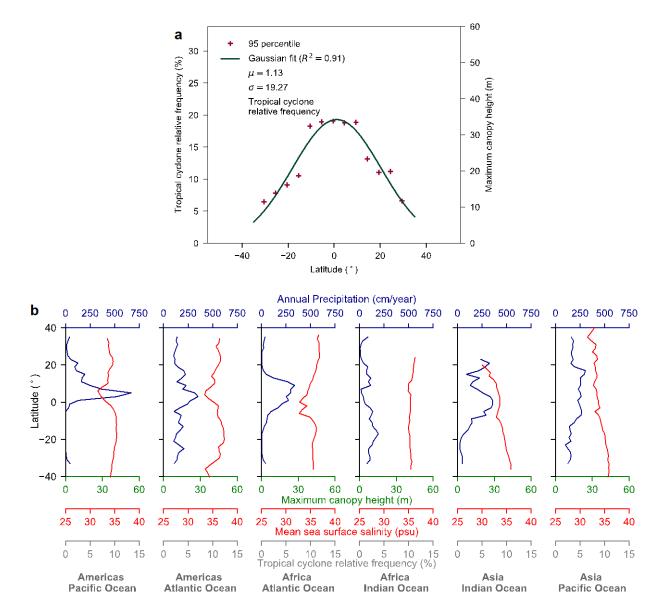
663

664

Figure 4 | Latitudinal variation of maximum canopy height (m) and global environmental variables. a, Relationship (black line) between latitude and maximum height (green circles) calculated on the 95th percentile of maximum height (red plus sign) (right y-axis) at every 5 degrees of latitude between about –30 and 30 degrees (i.e., where most mangroves occur). Tropical cyclone frequency (left y-axis) is shown in grey. **b**, Latitudinal trends in maximum canopy height (green bars), precipitation (blue line), SSS (red line), and cyclone relative frequency distribution (grey bins) along the major continental coastlines.

Tables

Table 1. Ten countries with the tallest maximum mangrove canopy height (a), and the largest total aboveground biomass (AGB) pools (b).

(a)	Country	Max height (m)	Mean height (m)	Max AGB (Mg/ha)	Mean AGB (Mg/ha)	Total AGB (Mg)	Total carbon (Mg)	Mangrove area (ha)
1	Gabon	62.8	23.5	910.5	244.0	33,578,276	61,504,323	137,597
2	Equatorial Guinea	57.7	21.6	800.0	208.6	2,630,892	5,337,399	12,613
3	Colombia	54.3	24.0	413.3	129.5	26,648,548	75,973,344	205,179
4	Venezuela	52.6	30.7	392.8	184.0	45,505,364	100,551,457	247,252
5	Panama	50.9	27.7	372.6	155.6	23,676,218	58,979,743	152,189
6	French Guyana	49.2	23.2	352.9	129.2	10,290,431	29,453,310	79,640
7	Cameroon	47.5	22.6	594.5	208.7	41,603,704	84,360,030	199,303
8	Angola	45.8	16.6	562.3	139.7	3,738,534	10,090,736	26,779
9	Costa Rica	45.8	23.4	314.7	116.4	4,512,007	13,998,836	38,752
10	Papua New Guinea	45.8	27.7	432.5	242.4	113,948,576	209,577,515	469,983

(b)	Country	Max height (m)	Mean height (m)	Max AGB (Mg/ha)	Mean AGB (Mg/ha)	Total AGB (Mg)	Total carbon (Mg)	Percent of global AGB
1	Indonesia	44.1	24.3	409.5	215.3	574,318,208	1,140,797,712	32.7
2	Papua New Guinea	45.8	27.7	432.5	242.4	113,948,576	209,577,515	6.5
3	Australia	25.5	11.9	212.6	119.4	112,797,816	342,085,251	6.4
4	Brazil	40.7	19.9	260.5	92.5	97,833,808	363,245,344	5.6
5	Malaysia	33.9	19.9	290.6	172.9	95,561,040	220,641,786	5.4
6	Bangladesh	25.5	15.4	421.2	171.7	73,916,552	171,532,878	4.2
7	Nigeria	33.9	13.4	355.3	96.5	66,791,716	240,715,439	3.8
8	Myanmar	30.5	13.7	257.3	130.7	61,974,552	175,266,415	3.5
9	Venezuela	52.6	30.7	392.8	184.0	45,505,364	100,551,457	2.6
10	Cameroon	47.5	22.6	594.5	208.7	41,603,704	84,360,030	2.4
	Total top 10 AGB					**1,284,251,336**	**3,048,773,825**	**73.2**